Impact of wheel shape on the vertical damage of cast crossing panels in turnouts

Y. Bezin, I. Grossoni & S. Neves
Institute of Railway Research, University of Huddersfield, Huddersfield, UK

ABSTRACT: Impact forces generated in the load transfer area of railway crossing panels lead to a range of degradation modes from wear and fatigue of the contacting materials, fatigue of supporting components to ballast/subgrade deterioration. A simplified modelling approach has been developed to first analyse the geometrical problem of the axle rolling through the crossing geometry, and in a second step to predict the vertical dynamic force produce from the interaction between the wheel unsprung mass and the track system. The force is analysed in the frequency domain to estimate the level of damage in different parts of the track system. A parametric analysis of wheel shapes was carried out showing that the axle lateral displacement has a significant influence on the produced level of damage and also that characteristics such as the wheel flange thickness and the equivalent slope in the area of contact also leads to increased damage. It is suggested that such a measure in combination with the simplified algorithms developed here could be used, possibly in combination with track side monitoring system, to highlight traffic instances leading to increased asset damage.

1 INTRODUCTION

Railway switches and crossings (S&C) are the most costly items for railway infrastructure managers. In the UK over 20% of the planned maintenance and renewal budget for 2014-19 is taken by S&C (Network Rail, 2014). Most development in railway crossing designs involves the use of advanced materials (e.g. improved Austenitic Manganese (Network Rail, 2002)), manufacturing technology (e.g. casting processes) and hardening processes (e.g. thermal flow and cooling). However the geometrical design and eventual machined shape of the running surface is based on practical machining capabilities and notional understanding of the compatibility between a theoretical set of a few wheel and the crossing shapes. The expectation is that the initial wear and plastic deformation under dynamic loads will quickly reshape the crossing surface geometry to better conform to the wheels of the traffic it sees. Yet the dynamic load generated between the wheel and the crossing at the transfer point (Jenkins et al., 1974) can vastly differ depending on the crossing designed geometry and the type of traffic running over. A systematic understanding of the effect of wheel shape on the damage mechanisms is not yet available. As part of the EU FP7 project SUSTRAIL, the University of Huddersfield developed a series of numerical simulation tools able to predict the effect of the geometrical interface between wheels and crossings (Bezin et al., 2014) for a large range of running conditions. Degradation mechanism involved with impact loads in the transfer area are poor ballast support, voided sleepers, transversal cracking of the casting, running surface damage (crossing nose and wing rail), heavy plastic deformation, material spalling and shelling. In this paper the methodology previously reported in (Bezin et al., 2014) is reviewed and a summary of the most influential parameters is provided. A critical analysis of the effect of wheel shape is then presented which in combination with the above simplified methodology offers a potential for condition based monitoring of S&C established on monitoring wheel geometrical characteristics.

2 METHODOLOGY AND NUMERICAL TOOLS

The modelling approach used for this work has been established within the project SUSTRAIL (Bezin et al., 2015) and previously presented in (Bezin et al., 2014). It was acknowledged at the start of the project that simulation methods for vehicle dynamic interaction at switches and crossings either based on available multibody system tools (Andersson et al., 2006, Lagos et al., 2012, Nicklisch et al., 2010) or more complex FE models (Markine et al., 2011, Pletz et al., 2012, Wan et al., 2014) have been used very successfully but are generally complex and time consuming, thus limiting the quantity of cases which can be simulated. This is particularly true with wheel population investigated, which constitute a significant contributor to the variation in predicted results. (Nielsen and Pålsson, 2012) employed 120 wheels using Latin Hypercube Sampling method to ensure a good representation of the wheel characteristics. This represents the largest sample used for a dynamic study so far. For all the above reasons it was decided in this study to limit the problem to the crossing panel and also focus only on the vertical dynamics while establishing a simple approach that would enable a larger range of cases to be taken into account, particularly the number of wheels.

2.1 *Kinematic axle motion*

In the first instance the crossing geometry is established from 3D CAD drawings and relevant cross sections saved into x-y coordinate at desired intervals along the crossing panel to allow accurate calculation of the wheel trajectory. Secondly the wheelset free kinematic movement is solved using the secondary differential equation 1, based on vehicle speed (v), initial distance between contact point (e), nominal wheel radius (r_0) and the rolling radius difference established between the crossing 3D layout and each wheel profile pairs of interest ($\Delta r(x,y)$). At each x-position along the panel, the point of contact on both wheels and the rails are estimated based on the shortest vertical distance between the wheel and rail profiles on either sides. Note that the friction and steering forces of the axle are ignored in this approach. The initial axle lateral displacement and angle of attack at the start of the crossing panel are given as input variables. The axle inertial mass and yaw stiffness are also ignored. Alternatively the program has been modified to force the axle in the fixed lateral and yaw angular position to understand better the range of possible motion of the axle through the crossing within the available gauge and check rail dimensions. The real motion of an axle will be somewhere between these two conditions of rigidly constrained and free rolling. Figure 1 shows the results of the wheel trajectory on the rolling radius map according to the two options. The results presented in this paper are based on the second option, and results are considered valid for vertical dynamics as long as the contact angle and resulting force component in the lateral direction are not significant.

$$\ddot{y} + v\text{^}2/(e.r_0\,)\,\Delta r(x,y) = 0 \tag{1}$$

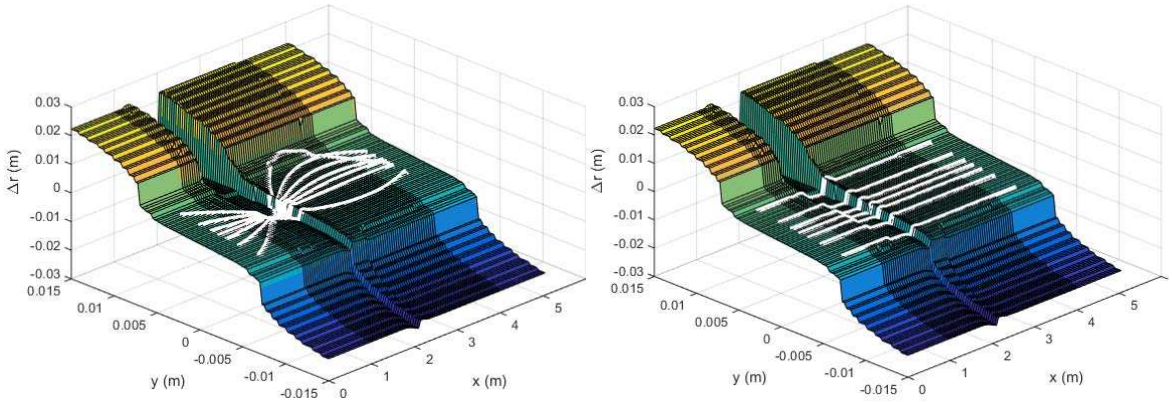

Figure 1. wheel trajectory on the rolling radius map; free kinematic motion (left) and constrained (right)

2.2 *Vertical wheel motion*

Based on the kinematic motion defined above and the resulting prediction of the contact point location on wheel and rails in dimension *x-y*, the vertical change of position of the wheel centre of gravity is estimated as per equation 2 (for the right wheel only, going through the crossing). Figure 2 shows the 3D CAD geometry and the various contact paths according to a range of lateral wheelset initial positions.

$$z_w(x) = z_r(x,y) + r_0 - \Delta r(x,y) \tag{2}$$

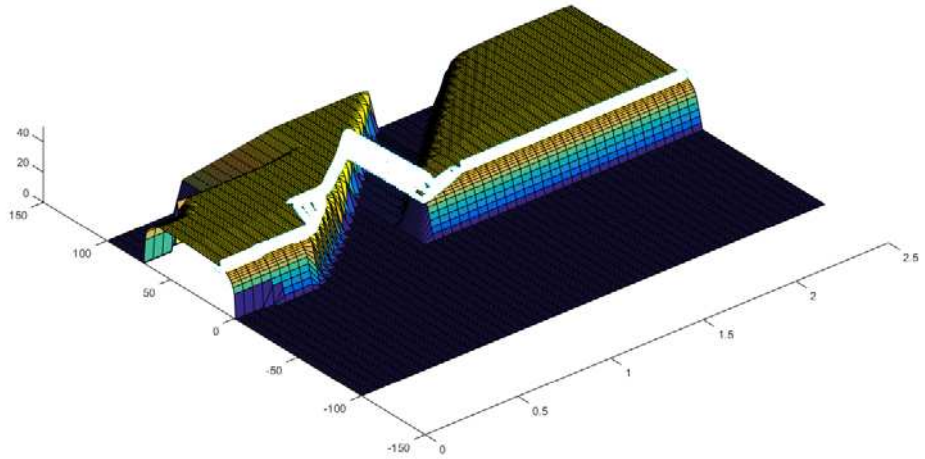

Figure 2. input 3D CAD geometry of a crossing and predicted contact path on the 3D surface based on a range of axle lateral positions.

2.3 *3 degree of freedom wheel-track mass system*

After the initial geometric problem described above is solved, the wheel vertical motion z_w is used as an input irregularity function between the wheel and the rail masses in a 3 degree of freedom (*dof*) mass-spring system representing the wheel unsprung mass and the track system with 2-dof (cast crossing and bearer/ballast masses). Figure 3 shows the representation of the 3-dof system and a range of representative input irregularities covering different wheelset lateral positions across the geometry. Triangular shapes are automatically detected to estimate the equivalent dip angle perceived by the wheel through the crossing. This is later used for results interpretation. Two methods are used, one to detect the angle in the vicinity of the lowest point and the other one to detect the global dip angle which would be equivalent to that measured on site using a straight edge device. Note however that here it is estimated based on the actual contact path of the wheel and can therefore vary with the wheelset lateral position and yaw angle.

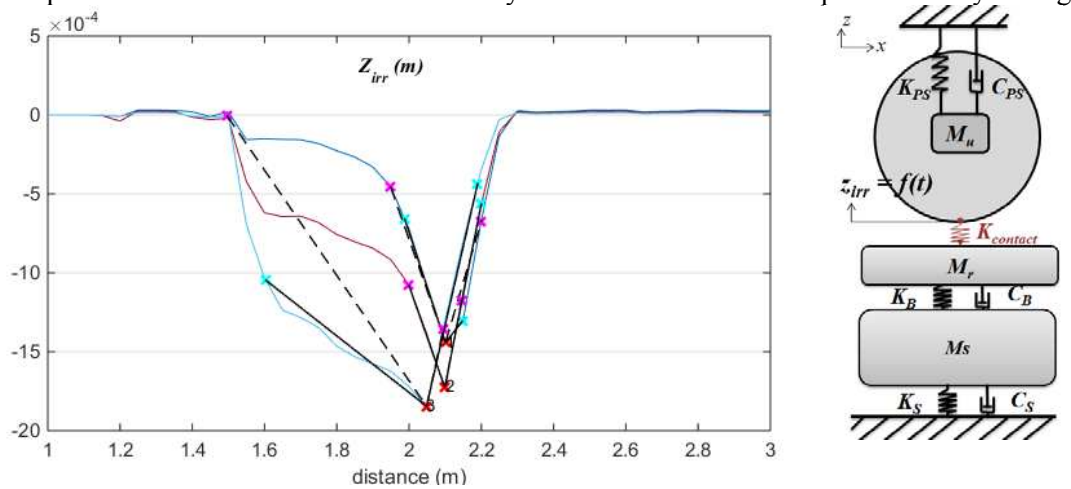

Figure 3. Calculated z_{irr} vertical irregularity (left) used as input to the 3DOF system model (left).

2.4 *Dynamic force prediction*

The contact is handled using a non-linear Hertzian approximation (Grossoni et al., 2014) and described in equation 3 below, allowing for loss of contact of the wheel. Where $F_{co}(t)$ is the contact force as a function of time, G_{co} is the Hertzian contact constant (Lei and Noda, 2002), z_r and z_w rail and wheel mass vertical motion respectively and $z_{irr}(t)$ the previously calculated input irregularity.

$$F_{co}(t) = \begin{cases} G_{co}^{-\frac{3}{2}} \cdot (z_w(t) - z_r(t) - z_{irr}(t))^{3/2} & if\, z_w(t) - z_r(t) - irr(t) > 0 \\ 0 & elsewhere \end{cases} \quad (3)$$

2.5 *Interpretation of results*

The output force predicted by the 3-dof model includes three principal frequencies which can be highlighted by applying a 5th order Butterworth low-pass filter as shown in Figure 4. Two cut-off frequencies are calculated as 1.5 times each of the lowest modal frequencies of the 3-dof model; the three main modes correspond to:

- Mode 1 (highest frequency): wheel mass moving out of phase with the crossing. Most of the energy goes into the contact between wheel and the crossing.
- Mode 2: (medium frequency): this is the wheel moving together with the rail mass against the bearer/ballast mass. Most of the energy goes into the crossing supporting elements and into bending strains. The contact and ballast also take a significant amount of strain energy.
- Mode 3 (lowest frequency): wheel unsprung mass coupled with the rail mass bouncing in phase with the bearer/ballast mass. Most of the energy is transmitted to the ballast, essentially leading to ballast settlement.

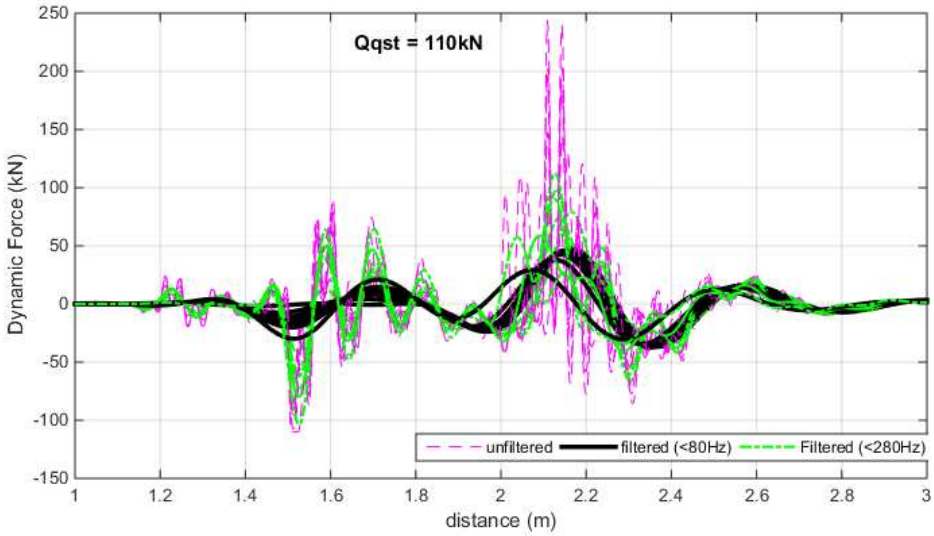

Figure 4. Dynamic forces for a range of lateral displacement with different levels of filtering: unfiltered-mode 1 (magenta lines), low-pass filtered <280Hz – mode 2 (green lines) and low-pass filtered <80Hz – mode 3 (thick black lines)

3 DEFINITION OF PARAMETRIC STUDY

The parametric study presented in this paper is concerned with the understanding of the variation of impact loading under the influence of the worn wheel shapes and the effective position of the wheel laterally as it negotiates the crossing. For this study a library of over 800 pairs of wheels measured on UK freight vehicles was used. First their characteristics were assessed in terms of commonly measured quantities such as flange height, flange thickness or wheel conicity. Then the entire population of wheel was used as input variable to the simplified 3-dof system

following the methodology described in the previous sections. Since the developed algorithm is very computationally efficient, a vast quantity of cases could be considered:

– One reference crossing: CEN56 1:91/4 half cant
– Two movement directions: facing, trailing
– A range of constrained wheel lateral positions spanning the range of possible motion
– Wheel population: 831 pairs of left and right wheels measured on freight axles
– Vehicle speed: a constant speed of 80 km/h was considered in this study

Previous results presented in (Bezin et al., 2014) showed that the direction of travel had little influence on the results. Other parameters of influence investigated were the vehicle speed, axle unsprung mass, the crossing angle and crossing geometry (Bezin et al., 2015). It was also shown that as the wheel moves towards the flange on the approach to the crossing, the likelihood of the force being significantly higher increases as does the variability in output results. This is shown in Figure 5. Based on the same set of results, this paper focuses from here onward on the further relationship between specific wheel shapes characteristics and the level of vertical damage observed.

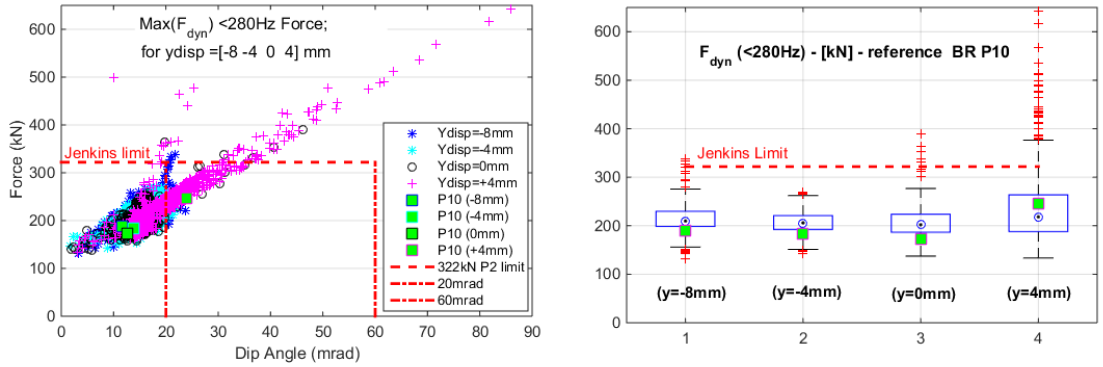

Figure 5. Low pass filtered (<280Hz) vertical peak force against equivalent dip angle (left plot) and statistical spread in results using box plots for each lateral input displacement (right plot). The square indicates the reference P10 profile

4 WHEEL POPULATION CHARACTERISTICS

Figure 6 shows the statistical measures collected based on all the various wheel shapes, showing an overlay of all wheel profiles. Standard measures are:

– Flange width (*Sd*)
– Flange height (*Sh*) 10mm below datum point (nominal radius)
– Flange angle distance (*qR*) between 2mm above flange tip and 10mm below datum point

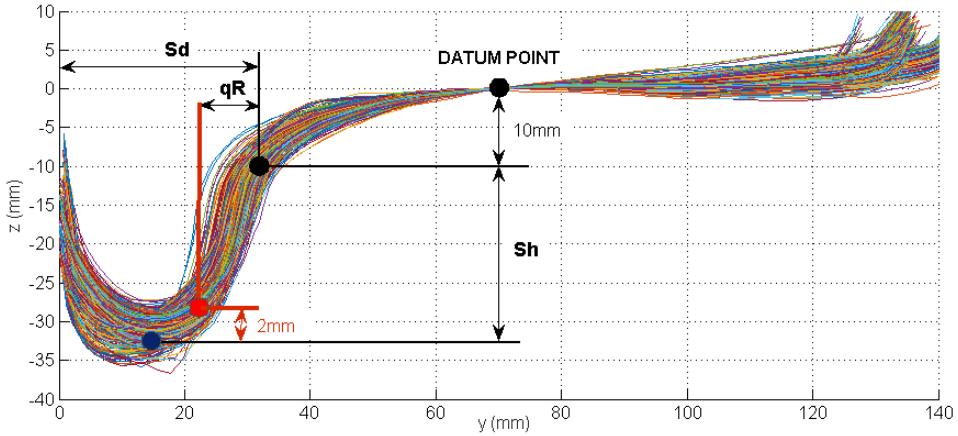

Figure 6. Population of wheel profiles showing standard statistic measures

The measures above are industry standard. It was decided to use additional measures (Figure 7) of the local profile slopes in different areas of the wheel representative of the contact conditions for (a) the wheelset running centrally aligned (straight running), (b) the wheel flange close to crossing nose (diverging route and opposite wheel close or in contact with check rail) and (c) the wheel away from the crossing (e.g. trailing axle in diverging routes):

- (a) Slope at nominal radius (70mm from flange back for UK P8 and P10) over a 20mm width
- (b) Slope 20mm away from nominal radius towards flange (50mm from flange back) over a 20mm width
- (c) Slope 20mm away from nominal radius towards field side (90mm from flange back) over a 20mm width

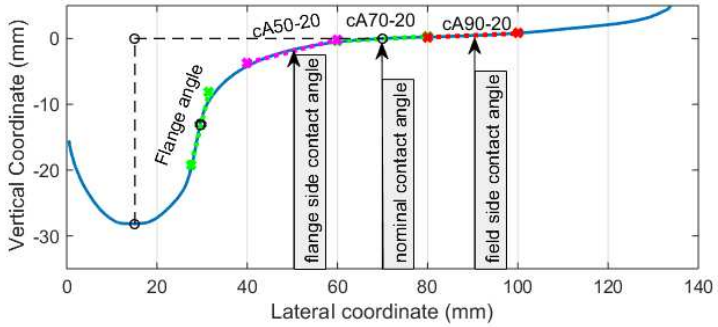

Figure 7. Additional wheel measures for local contact angles in different contact zones: cA50-20 (flange side), cA70-20 (nominal position) and cA90-20 (field side)

Population distributions regarding standard measures are presented in Figure 8, showing that the selected wheel population parameters follow a generalised extreme value distribution. New values for the P10 and worn limits are highlighted, showing that the flange thickness tends to spread around the initial new value as it wears out, while the flange height tends to increase as the wheel tread diameters gets thinner with wear. A small population of wheels is slightly over the standard recommended limit values.

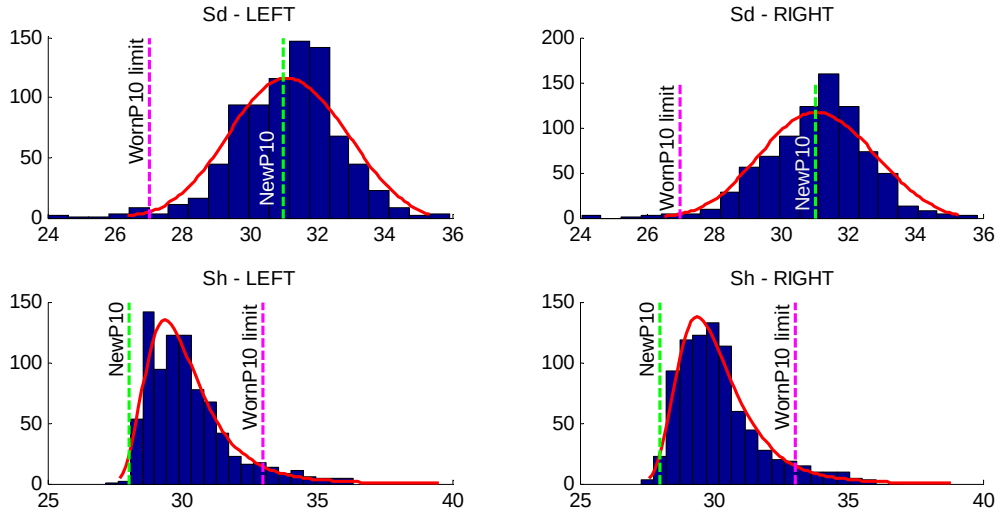

Figure 8. Wheel population statistical distribution: flange tickness (top) and flange height (middle) for left (left column) and right (right column) wheels

5 RESULTS ANALYSIS

5.1 *False flange wheels*

False flange wheel are commonly bad in terms of poor vehicle ride performance and therefore increase wear and tear of wheel and rails. As regards negotiating a crossing, it is shown here

that the false flange wheels generally lead to lower height drop (Figure 9 left) as the false flange maintains the wheel height over longer distances on the wing rail before contact on the crossing nose occurs, which incidentally appears to generate a population of wheels with lower vertical dynamic forces on average (Figure 9 right). Note that wing rail are often modified to include a groove in order to avoid other issues with the false flange contacting the field side of the wing rail and generating surface damage on that area.

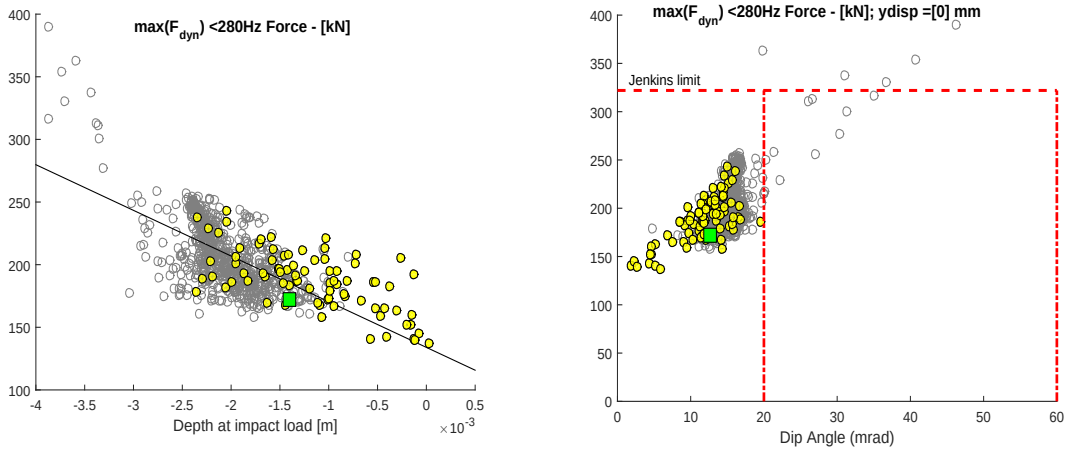

Figure 9. Dynamic peak forces (filtered <280Hz) against depth at impact (left) and against equivalent dip angle (right). Highlighted markers indicate wheels with false flange. Square for P10 reference wheel

5.2 *Increased conicity wheels*

In order to investigate the wheel population having an increased conicity, i.e. the slope angle at the nominal radius cA70-20 having a 50% increase from nominal 1:20 (or 0.05 rad) are highlighted in highlighted in Figure 10. This shows that all outliers ($F_{dyn} > 2.7\sigma$) belong to this category (with the exception of one wheel only). On general these wheels generate a larger dip angle and larger drop in height resulting in larger peak force. The same can be observed for the case where the wheel moves towards the field side and cA90-20 >0.05rad is highlighted (Figure 11) as well as when the wheel moves towards the flange and cA50-20 > $\mu_{cA50\text{-}20}+1.\sigma_{cA50\text{-}20}$ is highlighted (Figure 12).

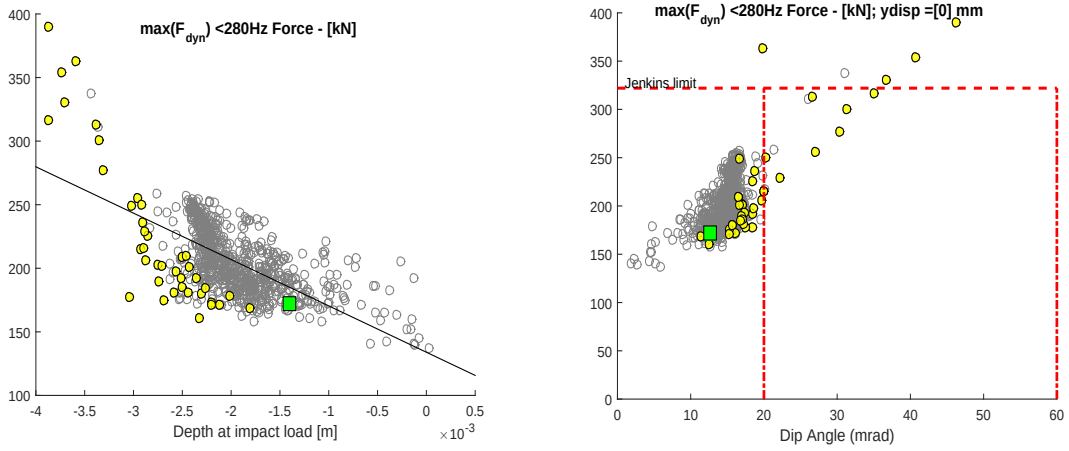

Figure 10. Dynamic peak forces (filtered <280Hz) against depth at impact (left) and against equivalent dip angle (right). highlighted markers indicate wheels with >50% increase conicity at nominal radius. Square for P10 reference wheel

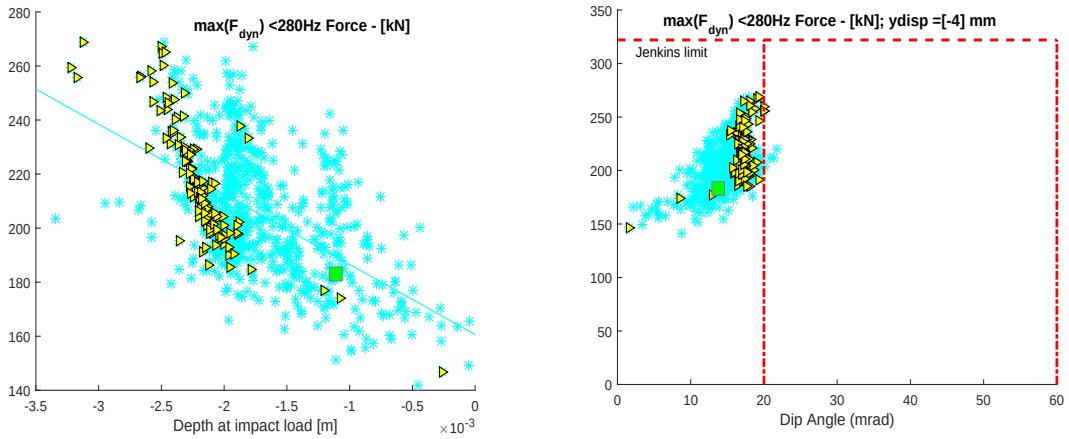

Figure 11. Dynamic peak forces (filtered <280Hz) against depth at impact (left) and against equivalent dip angle (right). Highlighted markers indicate wheels with increased conicity at nominal radius + 20mm. Square for P10 reference wheel

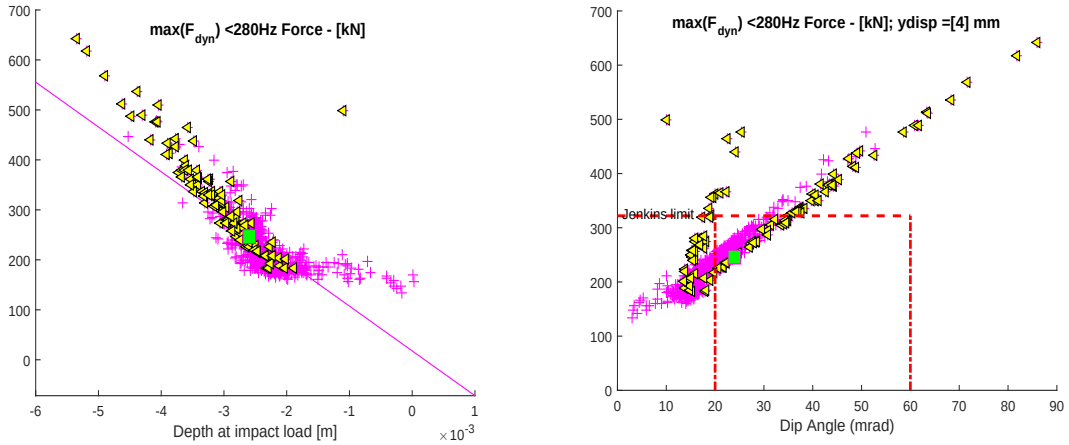

Figure 12. Dynamic peak forces (filtered <280Hz) against depth at impact (left) and against equivalent dip angle (right). Highlighted markers indicate wheels with increased conicity at nominal radius - 20mm. Square for P10 reference wheel

5.3 *Final observations on wheel geometry*

Finally this study demonstrate that based on specific wheel geometry characteristics, for example the flange thickness and the slope near the root of the flange as shown in Figure 13, these measures can be correlated between themselves and moreover the magnitude of the dynamic forces output can also be correlated. The plots show that as the wheel moves laterally closer to the crossing, then the wheels with the higher angled flange root and the thicker flange will clearly lead to higher impact loads. It was also observed during the project that in the specific cases where heavy crossing plastic flow in the lateral direction was observed (Figure 14) (deduced to be the result of heavy flange impact force), the track gauge was also a major contributory factor with a combined gauge narrowing and cross level defect observed locally around the crossing nose location (Figure 15).

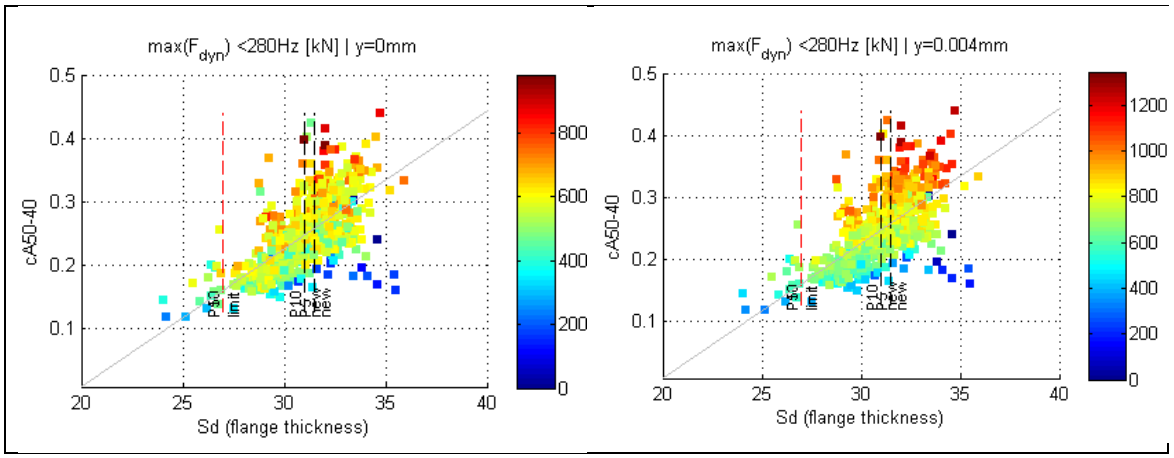

Figure 13. Dynamic peak forces (filtered <280Hz) as a function of flange thickness and slope near flange root (50mm from flange back) for y-disp = 0mm (left) and +4mm towards flange (right)

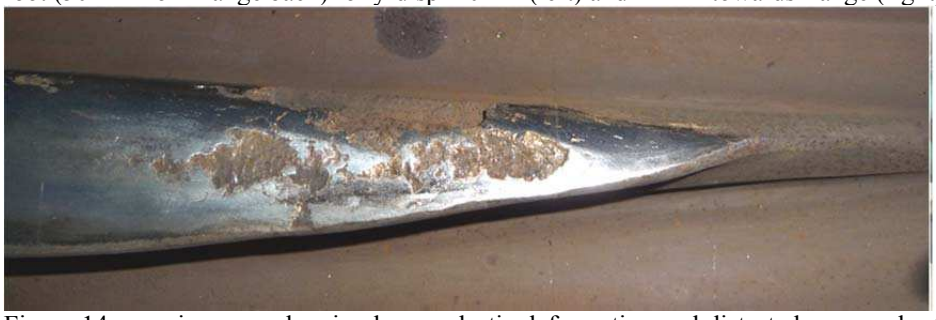

Figure 14. crossing nose showing heavy plastic deformation and distorted nose under the impact of passing wheels (non-compliance of wheel-crossing geometry)

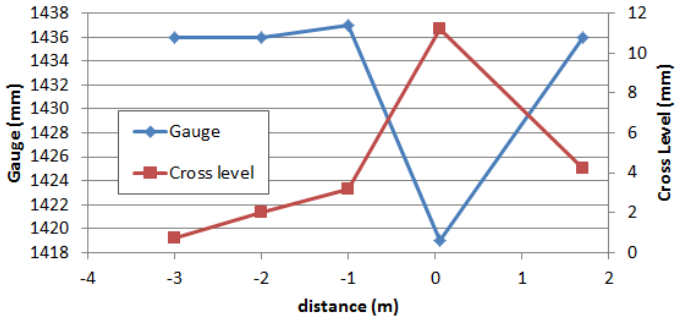

Figure 15. Gauge and cross level measurement for a crossing with nose damage

6 CONCLUSION AND FURTHER WORK

Simplified numerical models have been developed which allow the prediction of vertical damage to be derived from the dynamic force interaction of vehicle unsprung mass at a railway crossings panel. Using a stochastic approach the tool has been used to show the correlation between the damage in different levels of the track structure (contact, support components and ballast) and specific populations of wheel shape. In particular it was shown that the likeness of generating damage is linked to the lateral position of the wheels in the area of load transfer, in combination with flange thickness and the conical shape in the contact region. The higher the equivalent slope in the local area of contact, the higher the risk for vertical damage. The designed tool is extremely fast and developed algorithms can be further simplified and automated to envisage a practical application for S&C condition monitoring supported by traffic information such as the use of advanced automated wheel measurement systems which become more readily available. However it is acknowledged that a holistic approach needs to be taken whereby the track conditions also needs to be taken into account, particularly track gauge, cross level and check rail clearances in order to highlight problem areas.

The combined analysis of wheel geometry and track geometry tolerances needs to be developed further. The tool has also been further developed to include the full wheelset dynamic motion including steering forces to allow estimate of wear and rolling contact fatigue in the area of contact. This now requires full validation and will be coupled with full vehicle dynamic outputs to provide refined initial conditions for the axle lateral position and yaw angle as well as applying a lateral curving force in the turnout.

ACKNOWLEDGEMENT

The funding support of European Grant SCPO-GA-2011-265740 in support of the SUSTRAIL project is gratefully acknowledged.

REFERENCES

ANDERSSON, C., NIELSEN, J. & KASSA, E. 2006. Simulation of dynamic interaction between train and railway turnout. *Vehicle System Dynamics,* 44**,** 247-258.

BEZIN, Y., COLEMAN, I., GROSSONI, I., NEVES, S., HYDE, P., BRUNI, S., ALFI, S., RANTATALO, M., JÖNSSON, J., ASLAM, M., LAMBERT, R., BEAGLES, A., FLETCHER, D. & LEWIS, R. 2015. D4.4 Optimised switches and crossings systems, SUSTRAIL 265740 FP7.

BEZIN, Y., GROSSONI, I. & ALONSO, A. 2014. The Assessment of System Maintenance and Design Conditions on Railway Crossing Performance. *Proceedings of the 2nd International Conference on Railway Technology: Research, Development and Maintenance.* Civil-Comp Press, Stirlingshire, United Kingdom.

GROSSONI, I., BEZIN, Y. & ALONSO, A. 2014. Modelling Uneven Support at Railway Crossings using a Vehicle-track Coupling System. *Proceedings of the Second International Conference on Railway Technology: Research, Development and Maintenance.* Ajaccio, Corsica: Civil-Comp Press, Stirlingshire, United Kingdom.

JENKINS, STEPHENSON, CLAYTON, MORLAND & LYON 1974. The effect of track and vehicle parameters on wheel-rail vertical dynamic force. *the Railway Engineering Journal,* Vol 3, No1.

LAGOS, R. F., ALONSO, A., VINOLAS, J. & PÉREZ, X. 2012. Rail vehicle passing through a turnout: analysis of different turnout designs and wheel profiles. *Proceedings of the Institution of Mechanical Engineers, Part F: Journal of Rail and Rapid Transit,* 226**,** 587-602.

LEI, X. & NODA, N. A. 2002. Analyses of the dynamic response of vehicle and track coupling system with random irregularity of track vertical profile. *Journal of Sound and Vibration,* 258**,** 147-165.

MARKINE, V. L., STEENBERGEN, M. J. M. M. & SHEVTSOV, I. Y. 2011. Combatting RCF on switch points by tuning elastic track properties. *Wear,* 271**,** 158-167.

NETWORK RAIL 2002. Cast Austenitic Manganese Steel Crossings (formerly RT/CE/S/012).

NETWORK RAIL 2014. Renewal and Expenditure Summary, SBPT223.

NICKLISCH, D., KASSA, E., NIELSEN, J., EKH, M. & IWNICKI, S. 2010. Geometry and stiffness optimization for switches and crossings, and simulation of material degradation. *Proceedings of the Institution of Mechanical Engineers, Part F: Journal of Rail and Rapid Transit,* 224**,** 279-292.

NIELSEN, J. & PÅLSSON, B. 2012. Wheel-rail interaction and damage in switches and crossings. *Vehicle System Dynamics,* 50**,** 43-58.

PLETZ, M., DAVES, W. & OSSBERGER, H. 2012. A wheel passing a crossing nose: Dynamic analysis under high axle loads using finite element modelling. *Proceedings of the Institution of Mechanical Engineers, Part F: Journal of Rail and Rapid Transit,* 226**,** 603-611.

WAN, C., MARKINE, V. L. & SHEVTSOV, I. Y. 2014. Analysis of train/turnout vertical interaction using a fast numerical model and validation of that model. *Proceedings of the Institution of Mechanical Engineers, Part F: Journal of Rail and Rapid Transit,* 228**,** 730-743.